Journal of Microscopy

Journal of Microscopy, Vol. 273, Issue 3 2019, pp. 189–198 doi: 10.1111/jmi.12774
Received 15 July 2018; accepted 3 December 2018

ALPHABETA: a dedicated open-source tool for calculating TEM stage tilt angles

N. CAUTAERTS*,† , R. DELVILLE* & D. SCHRYVERS†
*Fuel Materials Group, Institute for Nuclear Materials Science, Mol, Belgium
†EMAT, Department of Physics, University of Antwerp, Antwerp, Belgium

Key words. Crystallography, diffraction, software, TEM, tilting, tool.

Summary

This work describes the concepts, the mathematical framework and the implementation of the open source ALPHABETA software, a dedicated tool for calculating α and β tilt angles on any TEM double tilt stage. ALPHABETA provides an intuitive user interface to calibrate the orientation of the region of interest and to subsequently calculate the angle tilts to reach a zone axis, to perform a rotation around a given reflection, or to set up a 2-beam or weak beam condition. The orientation of the sample on the stage and the tilt range reachable domain can be visualised in a stereographic projection plot. The accuracy of the method to reach a set of zone axis was evaluated and some case studies are presented. The tool significantly reduces time for tilting work as major tilts can be performed in image mode and reachable zones are beforehand indicated in the software. Besides facilitating the tilting to different zone axes, the software can be used for miscellaneous applications such as making dark field tilt series without specialised hardware.

Introduction

A time-consuming aspect of performing transmission electron microscopy (TEM) work on crystalline specimens is tilting the sample to the appropriate imaging conditions. Although double-tilt stages have become the standard for most TEMs used in the field of materials science, they are not the most intuitive for the work a microscopist needs to perform. For defect analysis, such as Burgers vector determination, an operator must tilt to multiple 2-beam conditions, which involves tilting out of zone axis in different directions making sure different rows of reflections stay excited. For crystallographic work, diffraction patterns along different zones are often required whereas for atomic resolution work, dedicated zones are needed.

The conventional strategy to tilting is following the Kikuchi lines in reciprocal space. This requires a skilled operator that is knowledgeable in their material and is working on large, low-defect crystals. However, for small grained, nanocrystalline, multiphase, or highly deformed material this can be challenging and time-consuming. As the operator tilts, the sample drifts and goes out of focus, causing the region of interest to stray from the field of view. Tilting is hence a slow incremental process comprised of switching between image mode (to correct drift and focus) and diffraction mode (to follow the tilting direction).

Calculation of tilt angles and computer-assisted tilting can overcome most of the limitations stated above by providing the user the tilt angles needed to reach the targeted orientations (typically a zone axis). With the advent of electron tomography (Weyland & Midgley, 2004; Midgley & Dunin-Borkowski, 2009), the demand for computer-assisted tilting has only increased. Specialised hardware and software that can perform automatic tilting and drift correcting is available from different manufacturers under different modalities ('Mel-Build', 2005; 'CrystalPack Module', 2017). For operators who wish to expand the capabilities of nonspecialised holders there exists KSpaceNavigator (Duden *et al.*, 2011) and Crystbox (Klinger & Jäger, 2015). KSpaceNavigator is specialised for tilting and stages can be modified to be controlled by it, but is not free and may require specialised hardware. Crystbox is freeware and provides many useful tools for microscopists. It includes a tilt angle calculation tool for zone axes, but it lacks some options a microscopist might find useful such as easily calculating orientations to 2-beam and weak beam conditions, manipulating multiple regions of interest with a different orientation and saving orientations. It is also not open source.

To address some of these shortcomings, a free, open source and user-friendly program named ALPHABETA was developed. It is dedicated to address all the tilting needs of a microscopist who does not have access to specialised hardware. A core principle was for the software to be flexible enough to adjust to multiple microscope settings (such as magnification and camera length, which may change the image rotation on

Correspondence to: N. Cautaerts, Fuel Materials Group, Institute for Nuclear Materials Science, SCK-CEN, Boeretang 200, BE-2400 Mol, Belgium. Tel: 014 33 3185; e-mail: niels.cautaerts@sckcen.be

the screen) and be able to switch between these settings on the fly. Without directly interacting with the microscope, the software calculates the tilt angles towards any arbitrary zone axis, 2-beam or weak-beam imaging condition in any crystalline material. This can save the operator valuable time. This paper describes the mathematical framework behind those calculations, something that is not readily available from the existing open literature, and gives a brief overview on the implementation. The accuracy of the method was evaluated and some case studies in which the software was successfully applied are presented.

Theory

Conventions

The ultimate goal of tilting a crystal is to orient its real or reciprocal space vectors in a particular way with respect to the electron beam. In order to calculate the required tilt angles of the stage, the transformation between vectors that the operator observes on the detector (in the form of a diffraction pattern or HRTEM image) and the actual crystal vectors must be fully described by matrix operations. Most of these operations are rotations; they are usually expressed by matrixes, the expressions of which are derived elsewhere (Bajd *et al.*, 2013). The multiple components that make up the entire transformation are described in Figure 1.

There are four transformations to convert the crystal coordinates (*hkl*) or [*uvw*] in reciprocal or real space, respectively, to detector coordinates that can be measured by the operator.

First, the crystal coordinates are converted to Cartesian coordinates in a coordinate system fixed to the crystal. This is achieved by left multiplying the crystal coordinates by a matrix M_{real} consisting of columns with the crystal basis vectors $\vec{a}$, $\vec{b}$ and $\vec{c}$ as described in this Cartesian system. The Cartesian system is defined such that its x-axis is parallel to real space vector $\vec{a}$, and such that the real space vector $\vec{b}$ lies in the x–y plane in the first or second quadrant when the angle between $\vec{a}$ and $\vec{b}$ is smaller than or larger than 90° respectively. Using these conventions, the matrix M_{real} that transforms [*uvw*] coordinates to $(x, y, z)_{\mathrm{car}}$ is given by Eq. (1). In the equations, a, b, and c are the lengths of the real space basis vectors and α, β and γ are the angles between $\vec{b}$ and $\vec{c}$, between $\vec{a}$ and $\vec{c}$, and between $\vec{a}$ and $\vec{b}$, respectively.

$$M_{real} = \begin{bmatrix} \vec{a} & \vec{b} & \vec{c} \end{bmatrix} = \begin{bmatrix} a & b\cos\gamma & c_1 \\ 0 & b\sin\gamma & c_2 \\ 0 & 0 & c_3 \end{bmatrix},$$

$$c_1 = c\cos\beta,$$

$$c_2 = \frac{cb\cos\alpha - cb\cos\beta\cos\gamma}{b\sin\gamma},$$

$$c_3 = \sqrt{c^2 - {c_1}^2 - {c_2}^2}. \qquad (1)$$

The reciprocal space basis vectors $\overrightarrow{a^*}$, $\overrightarrow{b^*}$ and $\overrightarrow{c^*}$ are defined as shown in Eq. (2) (De Graef & McHenry, 2007). The columns of the transformation matrix M_{recip} are comprised of these vectors. The reciprocal space basis vectors are described with respect to the same Cartesian system as the real space basis vectors.

$$\overrightarrow{a^*} = \frac{\vec{b}\times\vec{c}}{\vec{a}\cdot\left(\vec{b}\times\vec{c}\right)}, \quad \overrightarrow{b^*} = \frac{\vec{a}\times\vec{c}}{\vec{a}\cdot\left(\vec{b}\times\vec{c}\right)}, \quad \overrightarrow{c^*} = \frac{\vec{a}\times\vec{b}}{\vec{a}\cdot\left(\vec{b}\times\vec{c}\right)},$$

$$M_{recip} = \left[\overrightarrow{a^*}\,\overrightarrow{b^*}\,\overrightarrow{c^*}\right]. \qquad (2)$$

Cartesian coordinates can be transformed back to crystal vectors by left multiplying by the inverse of M_{recip} and M_{real}, depending on whether reciprocal or real space coordinates are desired.

The 'stage' and its coordinate system should be thought of as the plane on which the macroscopic sample rests. The crystal under investigation will have a particular fixed orientation with respect to the stage. This orientation is described as the transformation matrix R_{ori} which converts the Cartesian coordinates from the crystal to the stage coordinates. Because both these coordinate systems are Cartesian, R_{ori} is a rotation matrix with a number of special properties such as ${R_{ori}}^{-1} = {R_{ori}}^{T}$. Finding this matrix in a practical way is described in the next subsection.

Once a vector is described with respect to the coordinate system fixed to the stage, it can be transformed to what in this paper will be considered 'absolute' coordinates by rotation matrix R_{rot}. The absolute coordinate system is defined such that the stage coordinate system aligns with it when the tilt angles are both zero and the sample is horizontal. The X_{abs} axis aligns with the holder's longest dimension, pointing away from the sample, along the holder, away from the holder's handle. The Z_{abs} axis is defined to lie along the optical axis of the microscope, pointing down. The Y_{abs} axis is defined according to the right handed convention such that $X_{abs} \times Y_{abs} = Z_{abs}$. After tilting, the stage coordinate system will deviate from the absolute coordinate system in the following way: the Y_{sta} system will be rotated by an angle α away from Y_{abs} along rotation vector X_{abs}, and X_{sta} will be rotated by an angle β away from X_{abs} along rotation vector Y_{sta}. Note that stage angles α and β are not related to the angles between the crystal basis vectors but share the same symbols. The rotation matrix R_{rot} is hence described as a compound rotation, of first β around Y_{abs} then α around X_{abs} as shown in Eq. (3). A combination of rotations is still a rotation, so ${R_{rot}}^{-1} = {R_{rot}}^{T}$. Another interpretation of R_{rot} is that the columns represent the stage coordinate basis vectors as described in the absolute coordinate system.

$$R_{rot} = \begin{bmatrix} 1 & 0 & 0 \\ 0 & \cos\alpha & -\sin\alpha \\ 0 & \sin\alpha & \cos\alpha \end{bmatrix} \begin{bmatrix} \cos\beta & 0 & \sin\beta \\ 0 & 1 & 0 \\ -\sin\beta & 0 & \cos\beta \end{bmatrix}$$

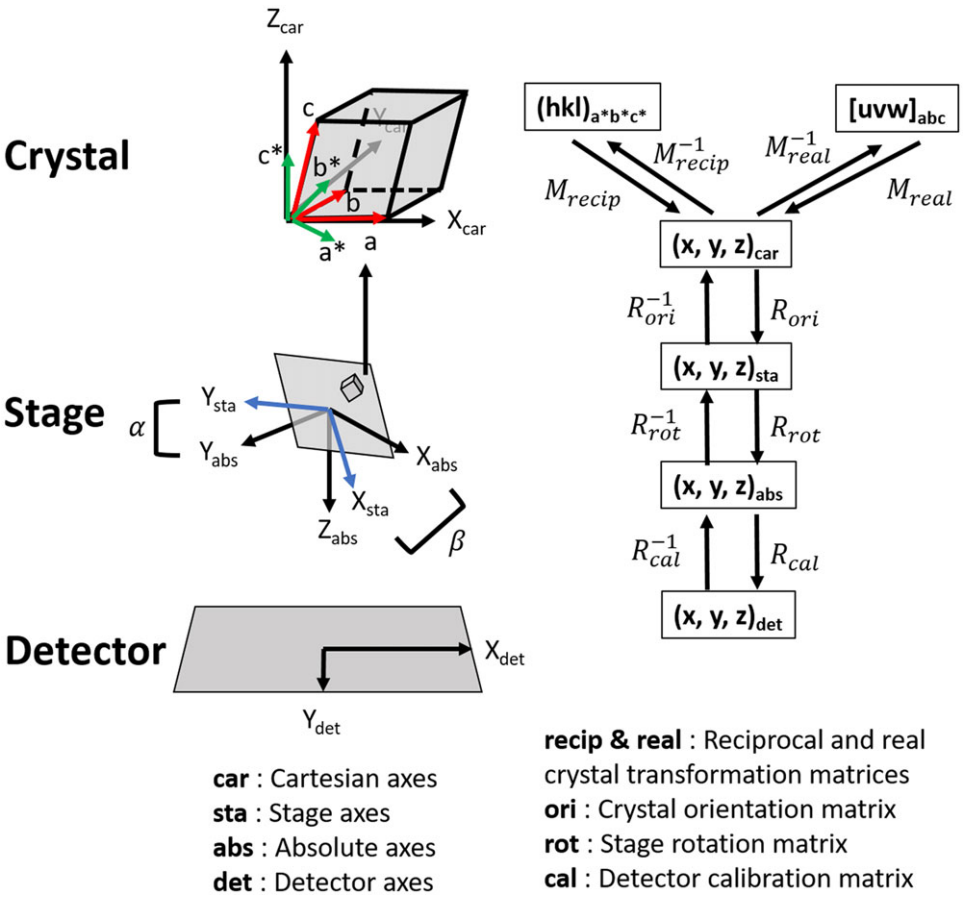

Fig. 1. Pictorial representation of the conventions adopted in this work to represent vectors and orientations. The transformation from crystal vectors, reciprocal (*hkl*) or real [*uvw*], to detector vectors that the operator can measure happens through three intermediary frames of reference: the Cartesian coordinate system fixed to the crystal, the stage coordinate system fixed to the plane of the stage and the 'absolute' coordinate system of the microscope.

$$= \begin{bmatrix} \cos\beta & 0 & \sin\beta \\ \sin\alpha\sin\beta & \cos\alpha & -\sin\alpha\cos\beta \\ -\cos\alpha\sin\beta & \sin\alpha & \cos\alpha\cos\beta \end{bmatrix}. \quad (3)$$

The final step is the transformation of absolute coordinates to detector coordinates. The detector coordinate system is defined such that when looking straight at the detector image, X_{det} points to the right, Y_{det} points downwards and Z_{det} points into the image. Z_{abs} and Z_{det} will always be aligned, so only the direction of the X_{abs} axis on the screen must be established. For this, a specific detector rotation calibration must be performed, which is detailed below. Once the angle θ between X_{abs} and X_{det}, both lying in the horizontal plane, is established, the transformation matrix R_{cal} to go from absolute to detector coordinates is given by Eq. (4). In older TEM instruments, the image or diffraction pattern rotates with magnification or camera length which changes θ. This was taken into consideration in ALPHABETA; a list of calibration angles for different settings can be supplied. The angle θ can be determined by tracing the motion of Kikuchi line intersections in the diffraction pattern when tilting over the α axis. Other strategies can also be employed, which are detailed in the user manual.

$$R_{cal} = \begin{bmatrix} \cos\theta & -\sin\theta & 0 \\ \sin\theta & \cos\theta & 0 \\ 0 & 0 & 1 \end{bmatrix}. \quad (4)$$

Calculating the crystal orientation

The orientation matrix R_{ori} that transforms crystal coordinates to stage coordinates can be calculated by coupling three known crystal vectors to known detector vectors considering that all the other transformations are known. This is most easily accomplished by tilting the crystal to a zone axis [*uvw*]. When this condition is met, the zone axis crystal vector is aligned with the detector Z-axis. Reciprocal space vectors will be in the detector *X*–*Y* plane and will be visible on the screen in the form of diffraction spots. One arbitrarily chosen reflection (*hkl*), measured to be lying at angle φ with the *X*-axis of the detector, constitutes a second vector. This vector is by definition perpendicular to the zone axis. A third vector can be found perpendicular to the zone and the reflection; this vector will also

lie in the detector X–Y plane but will not necessarily coincide with a reflection. Once these vectors are transformed to Cartesian coordinate vectors and normalised, they can be used to construct a transformation matrix that maps the unit vector parallel to the zone to the vector [001], the unit vector parallel to the reflection to $[\cos\varphi,\ \sin\varphi,\ 0]$, and the unit vector normal to these vectors to $[\cos(\varphi+\frac{\pi}{2}),\ \sin(\varphi+\frac{\pi}{2}),\ 0]$. This process is shown in Eq. (5). The overall transformation matrix R can be decomposed into its constituents (see Fig. 1) and from this, R_{ori} can be calculated. All matrixes are orthogonal matrices, so their transpose is their inverse.

$$\begin{aligned}
&\overrightarrow{Z_{car}} = M_{real}\begin{bmatrix}u\\v\\w\end{bmatrix},\ \overrightarrow{R_{car}} = M_{recip}\begin{bmatrix}h\\k\\l\end{bmatrix},\ \overrightarrow{N_{car}} = \overrightarrow{Z_{car}} \times \overrightarrow{R_{car}},\\
&R_s = \begin{bmatrix}\frac{\overrightarrow{Z_{car}}}{\left\|\overrightarrow{Z_{car}}\right\|} & \frac{\overrightarrow{R_{car}}}{\left\|\overrightarrow{R_{car}}\right\|} & \frac{\overrightarrow{N_{car}}}{\left\|\overrightarrow{N_{car}}\right\|}\end{bmatrix},\\
&R_d = \begin{bmatrix}0 & \cos\varphi & \cos\left(\varphi+\frac{\pi}{2}\right)\\ 0 & \sin\varphi & \sin\left(\varphi+\frac{\pi}{2}\right)\\ 1 & 0 & 0\end{bmatrix},\\
&R_{cal}R_{rot}R_{ori}R_s = R_d\\
&R_{ori} = R_{rot}^T R_{cal}^T R_d R_s^T
\end{aligned} \tag{5}$$

vector becomes aligned with the Z-axis of the detector. This problem is expressed in Eq. (6). R_{cal} is not required in the equation because the absolute Z-axis always remains parallel to the detector Z-axis. Zone axes are usually expressed in real space coordinates $[uvw]$, but any crystal direction can be rotated onto the Z-axis; ALPHABETA allows reciprocal space vectors (hkl) as input as well.

$$\begin{aligned}
v_{sta} &= R_{ori}\ M_{real}\begin{bmatrix}u\\v\\w\end{bmatrix},\\
R_{rot,\ calc\ \frac{v_{sta}}{\|v_{sta}\|}} &= \begin{bmatrix}0\\0\\1\end{bmatrix}.
\end{aligned} \tag{6}$$

In ALPHABETA, the solution to this system is calculated numerically, but an analytical solution is also possible.

Calculating tilt angles to rotate around a reflection

A tilt series around a particular reflection (hkl) may be desirable. This may be achieved by using the general rotation axis-angle matrix formalism $R_{axis-angle}$ as shown in Eq. (7). A diagram of the process is shown in Figure 2.

$$R_{axis-angle}\left(\begin{bmatrix}u_x\\u_y\\u_z\end{bmatrix},\theta\right) = \begin{bmatrix}\cos\theta+u_x^2(1-\cos\theta) & u_xu_y(1-\cos\theta)-u_z\sin\theta & u_xu_z(1-\cos\theta)+u_y\sin\theta\\ u_xu_y(1-\cos\theta)+u_z\sin\theta & \cos\theta+u_y^2(1-\cos\theta) & u_yu_z(1-\cos\theta)-u_x\sin\theta\\ u_xu_z(1-\cos\theta)-u_y\sin\theta & u_yu_z(1-\cos\theta)+u_x\sin\theta & \cos\theta+u_z^2(1-\cos\theta)\end{bmatrix}. \tag{7}$$

Once R_{ori} is found, the orientation of the crystal on the stage is completely determined and tilt angles can be calculated as in the following sections.

The caveat is that the indexation must be performed correctly: the original zone axis and chosen reflection must be correctly identified. Even if the operator is knowledgeable about the crystal system, a selected area diffraction pattern will usually include 180° ambiguity. All diffraction patterns show 2-fold rotation symmetry, whereas most zones of a crystal do not. To overcome these difficulties, ALPHABETA has a built-in indexation tool, as well as a test function in order to remove the ambiguity. This test function involves calculating tilt angles to another zone axis assuming the indexation of the user is correct. If the zone is not found, then the indexation is not correct; hence the operator will know to rotate the indexation by 180°.

Calculating tilt angles to go to another zone

To tilt to another zone, the parameters α and β in the rotation matrix R_{rot} must be calculated such that a particular crystal

The Cartesian representation of the unit vector pointing towards the reflection $[u_x,\ u_y,\ u_z]$ is used as rotation axis in $R_{axis-angle}$. Tilting by θ around this vector will put the vector at $-\theta$ tilt from the zone axis onto the zone. So, the vector at $-\theta$ must be found by rotating the current zone by $-\theta$ over the rotation vector, then converted to stage coordinates. Calculating the alpha and beta to put this vector onto the zone axis is a problem identical to the problem of tilting to another zone axis (Eq. (6)).

$$\begin{aligned}
\begin{bmatrix}u_x\\u_y\\u_z\end{bmatrix} &= \frac{M_{recip}\begin{bmatrix}h\\k\\l\end{bmatrix}}{\left\|M_{recip}\begin{bmatrix}h\\k\\l\end{bmatrix}\right\|},\\
v_{sta} &= R_{ori}\ R_{axis-angle}\left(\begin{bmatrix}u_x\\u_y\\u_z\end{bmatrix},-\theta\right)M_{real}\begin{bmatrix}u\\v\\w\end{bmatrix},\\
R_{rot,calc\ \frac{v_{sta}}{\|v_{sta}\|}} &= \begin{bmatrix}0\\0\\1\end{bmatrix}.
\end{aligned} \tag{8}$$

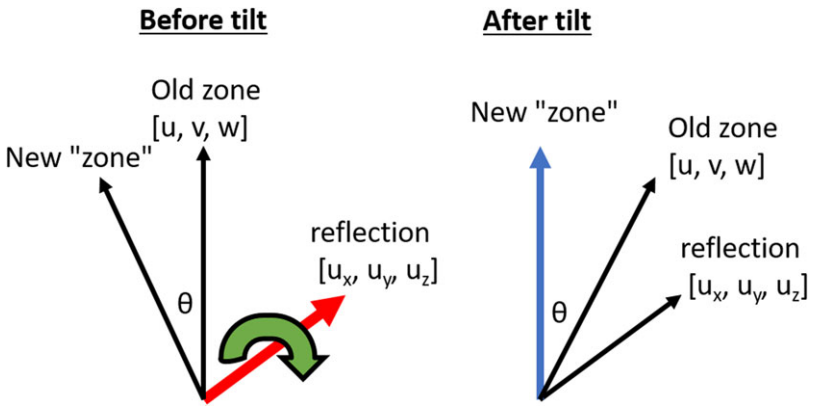

Fig. 2. Diagram of tilting around a reflection. The new 'zone' and old zone are both perpendicular to this reflection. Using the reflection as rotation vector, the new zone is at $-\theta$ from the old zone axis before the tilt of θ. The new 'zone' is in quotes because it is unlikely this vector can be expressed by integer members.

Naturally, for this method to work, an initial zone axis $[uvw]$ and a perpendicular reflection (hkl) (acting as a rotation vector) must be supplied.

Calculating tilt angles to go to a 2-beam condition

This is a variation on the problem of calculating a tilt around a reflection. Usually, when an operator wants to achieve the $\vec{g}$ 2-beam condition, the aim is to excite $\vec{g}$ and have the reflection centred on the optical axis. Here, $\vec{g}$ represents a reciprocal lattice vector (hkl) and this imaging condition is also known as centred dark field (CDF) imaging. To achieve this, the sample must be tilted 8–10° out of zone axis around $\vec{g}$ and subsequently such that reflection $-\vec{g}$ lies on the Ewald sphere. Then the beam must be tilted to bring $\vec{g}$ on the optical axis. The additional tilt towards $-\vec{g}$ can be calculated from geometric considerations as seen in Figure 3. The sample tilt φ required to bring $-\vec{g}$ on the Ewald sphere is the complement angle of the angle between K_0 and $-\vec{g}$: $\varphi = \frac{\pi}{2} - \cos^{-1}\left(\frac{\|-\vec{g}\|}{\|2\ K_0\|}\right)$.

Finding the vector to tilt onto the optical axis can then be summarised as shown in Figure 4 and Eq. (9). The chosen reflection is converted to Cartesian coordinates and normalised. This is the first rotation axis $[u_x, u_y, u_z]$ that is used to rotate the zone axis, also converted to Cartesian coordinates and normalised, by θ (8–10°) to keep only one line of reflections excited. A second rotation axis $[t_x, t_y, t_z]$ is then defined by the cross product between the first rotation axis and the new vector on the optical axis $v_{car,2}$. This vector is then rotated again away from the optical axis by φ around the second rotation axis. Finally, this vector is converted to the right coordinate system and the α and β are calculated by solving the system as before. Again, the vector to be brought onto the optical axis must be found by performing 'inverse' rotations on the initial zone axis.

$$
\begin{aligned}
\begin{bmatrix} u_x \\ u_y \\ u_z \end{bmatrix} &= \frac{M_{recip}\begin{bmatrix} h \\ k \\ l \end{bmatrix}}{\left\| M_{recip}\begin{bmatrix} h \\ k \\ l \end{bmatrix} \right\|}, \\
v_{car,2} &= R_{axis-angle}\left(\begin{bmatrix} u_x \\ u_y \\ u_z \end{bmatrix}, -\theta\right) \frac{M_{real}\begin{bmatrix} u \\ v \\ w \end{bmatrix}}{\left\| M_{real}\begin{bmatrix} u \\ v \\ w \end{bmatrix} \right\|}, \\
\begin{bmatrix} t_x \\ t_y \\ t_z \end{bmatrix} &= \begin{bmatrix} u_x \\ u_y \\ u_z \end{bmatrix} \times v_{car,2}, \\
v_{sta} &= R_{ori}\ R_{axis-angle}\left(\begin{bmatrix} t_x \\ t_y \\ t_z \end{bmatrix}, -\varphi\right) v_{car,2}, \\
R_{rot,\ calc} v_{sta} &= \begin{bmatrix} 0 \\ 0 \\ 1 \end{bmatrix}. \qquad (9)
\end{aligned}
$$

Once the operator has tilted $-\vec{g}$ to Bragg orientation, the beam tilts can be used to bring $\vec{g}$ onto the optical axis.

Calculating tilt angles to go to a weak-beam condition

Tilting to weak beam conditions is analogous to tilting to 2-beam conditions. The difference is the value of the additional tilt angle φ. The situation is described in Figure 5. After tilting sample and beam, the operator wants to image with reflection $k\vec{g}$ and have $n\vec{g}$ on the Ewald sphere (in the case of the figure, $k = 1$ and n is about 3). The imaging reflection coefficient k is always an integer and usually 1, n can be any real number;

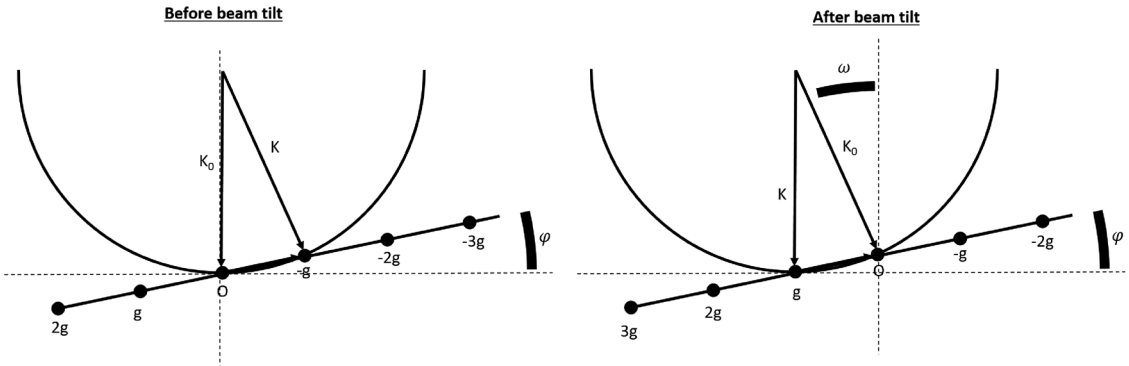

Fig. 3. On the left, the geometry of the $-g$ 2-beam tilting condition. When g is brought to the optical axis by tilting the beam, it will be in Bragg orientation. Angles in the figure are highly exaggerated.

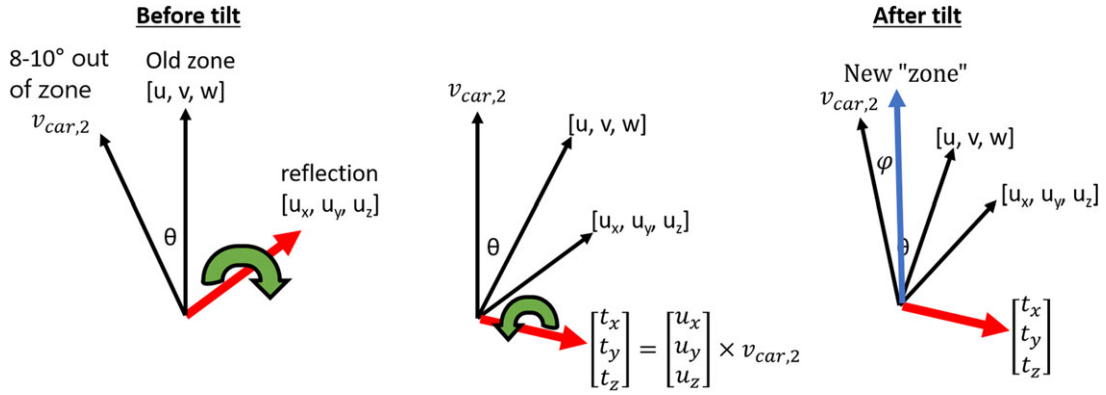

Fig. 4. The tilting scheme used for calculating 2-beam and weak-beam conditions. The first tilt is identical to the case of tilting around a reflection: to tilt to a 2-beam condition, the operator must tilt 8–10° out of zone axis first, keeping the row of reflections of interest excited. After this tilt, an additional tilt of φ must be performed to tilt the row of reflections towards the optical axis.

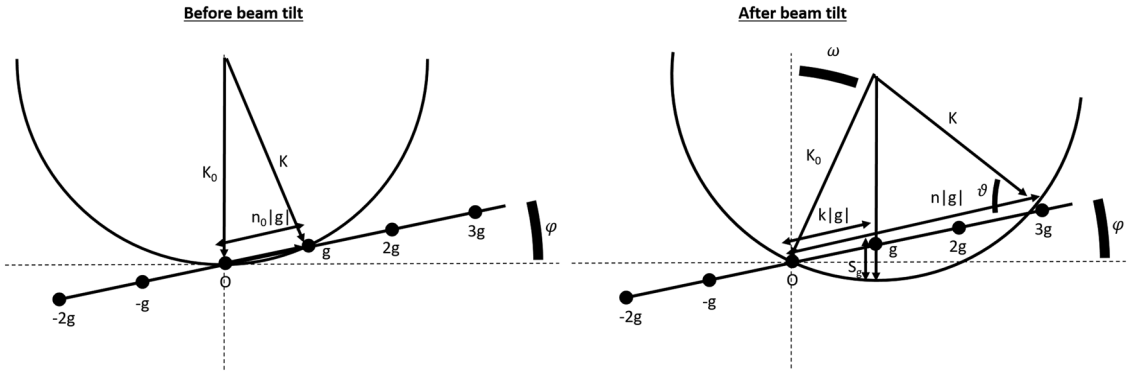

Fig. 5. On the left, the geometry of the n$_0$g tilting condition when the beam is not tilted. When kg (in the figure $k = 1$) is brought to the optical axis by tilting the beam, the ng weak beam condition will be achieved with a geometric excitation error S_g. Angles in the figure are highly exaggerated.

some sources suggest a noninteger n is even preferable as long as the excitation error S_g is larger than 2×10^{-6} nm^{-1} (Jenkins & Kirk, 2000).

The goal is to calculate sample tilt angle φ given a desired k and n. The angle between K_0 and the row of reflections after the beam tilt is $\vartheta = \cos^{-1}\left(\frac{n\|\vec{g}\|}{2\|K_0\|}\right)$. The required sample tilt to have $k\vec{g}$ on the optical axis after beam tilt can then be calculated considering that $\|\overrightarrow{K_0}\| \cos(\vartheta + \varphi) = k\|\vec{g}\| \cos\varphi$. Once φ is solved, the same calculation can be performed as in the 2-beam case (see Eq. (9)). After the sample is tilted but before the beam tilt, $n_0\vec{g}$ will cross the Ewald sphere. Then the operator needs to use the beam tilts to bring reflection $k\vec{g}$

onto the optical axis such that the $n\vec{g}$ weak beam condition is achieved.

Materials and methods

ALPHABETA was implemented in Python using common linear algebra, plotting and user interface libraries. An overview snapshot of the user interface can be seen in Figure 6. The details of the user interface and working with the program are described in the user manual, which can be downloaded together with the program or as the supplementary materials file accompanying the electronic version of this paper. ALPHABETA is free for download at https://github.com/din14970/ALPHABETA-TEM-tilting-suite/releases.

For evaluating the accuracy, a monocrystalline Si specimen was used. For the application demonstration, the material used was a heavily cold worked Ti-stabilised austenitic stainless steel that was heat treated at 800°C. The material is a cubic structure with lattice parameter 3.6 Å. Due to the heat treatment, fine Ti–C nanoprecipitates with lattice parameter 4.2 Å are dispersed throughout the grains on the dislocations. These share a cube-on-cube orientation relationship with the matrix and hence ideal for testing various dark field configurations.

The microscope used for the work was a Jeol 3000F equipped with a Schottky FEG source. The observations were all made on a slow scan CCD camera. In the diffraction pattern, the alpha axis was found to be calibrated at $\theta = 314°$ with the detector X-axis, independent of camera length.

Results and discussion

Evaluation of tilting accuracy

The calculations described in the previous section are exact for the crystal. The tilting accuracy depends entirely on the stage tilt accuracy and the initial calibration accuracy with the following uncertainties:

- Detector angle calibration uncertainty ($\theta \pm \delta_\theta$)
- Crystal orientation angle uncertainty ($\varphi \pm \delta_\varphi$)
- Stage tilt angle uncertainty ($\alpha \pm \delta_\alpha$ and $\beta \pm \delta_\beta$) due to stage backlash and nonlinearities

It is assumed that the operator can position the sample in an initial perfect zone axis orientation.

The influence of the different sources of uncertainty in the initial crystal orientation on the error in the calculated result can be estimated by propagating the errors. Some simplifications and assumptions need to be made. Assume the most simple case of a cubic crystal with lattice parameter 1 (such that the crystal systems and the Cartesian systems are identical), sitting on the stage at tilts $\alpha = 0$ and $\beta = 0$ with the [001] zone axis aligned with the electron beam and the [100]

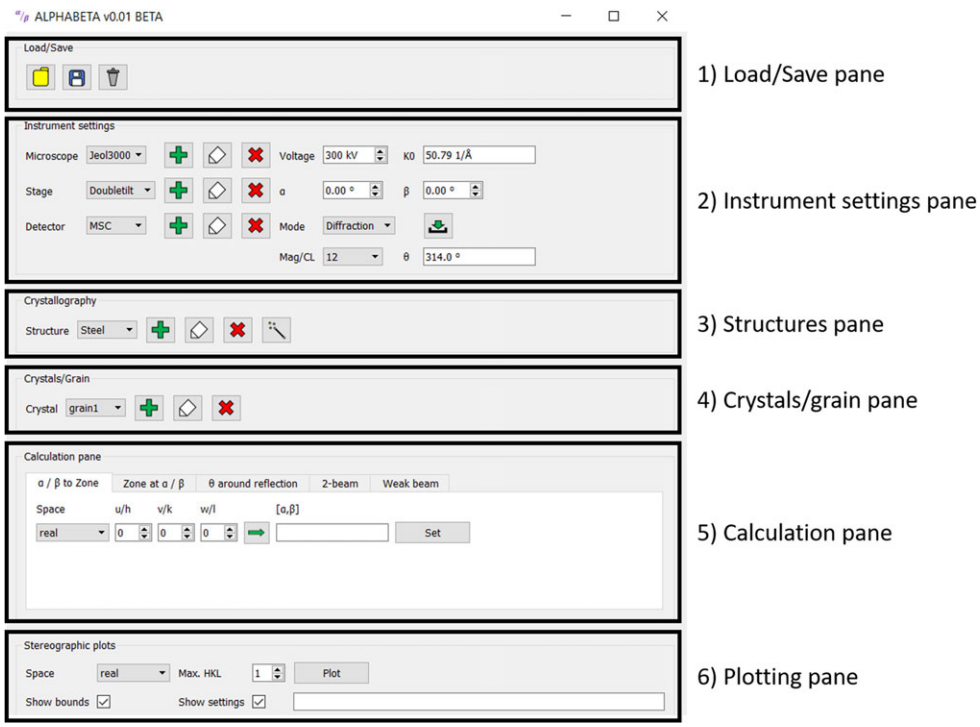

Fig. 6. ALPHABETA user interface overview.

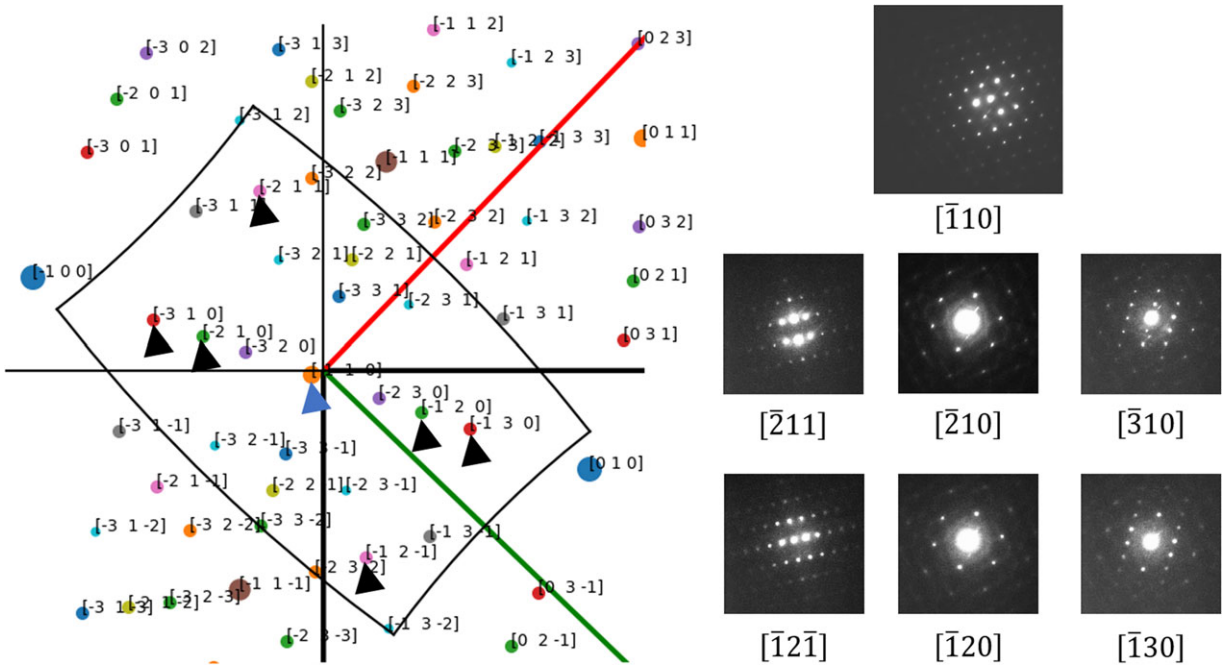

Fig. 7. On the left, the orientation of the Si crystal plotted in stereographic projection as determined in the experiment. The red and green lines indicate the directions of the α and β axis, respectively. The black shape represents the boundary of stage tilting. The black arrows indicate the zones used to test the influence of the stage nonlinearities. On the right are the diffraction patterns taken in these zones. The angles where perfect zone axis was achieved were recorded and compared to the calculated values.

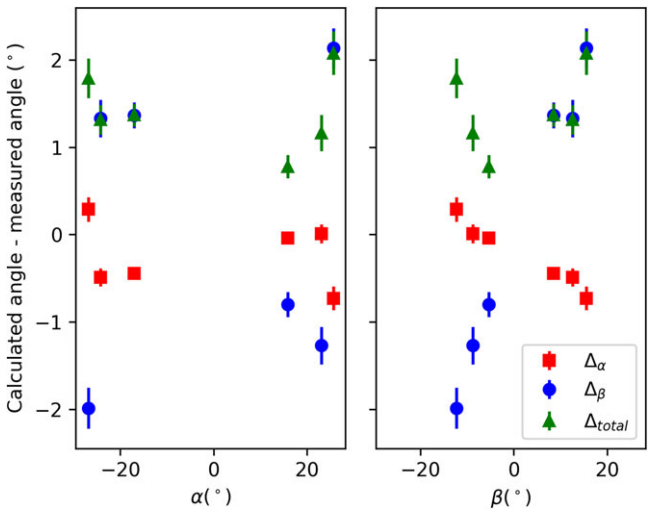

Fig. 8. Absolute error between calculated stage angles and experimentally observed stage angles to reach the different zones indicated in Figure 7, plotted versus the experimentally determined α and β angles. The total difference angle is the angle between the desired zone axis and the vector that is expected to be on the optical axis according to the calculations at the experimental tilt angles. The error bar represents the error resulting from the uncertainty in calibration angle φ.

aligned with the α axis. Also assume the detector angle $\theta = 0$. This represents the ground truth, but the measurements of these starting angles are slightly perturbed with a small angles δ_i. Using the sum of angle identities and the linearisation approximation for small angles, the sines and cosines in the matrix expressions can be simplified with expressions $\sin(\theta \pm \delta) \approx \sin\theta \pm \delta\cos\theta$ and $\cos(\theta \pm \delta) \approx \cos\theta \mp \delta\sin\theta$. Terms with a higher order than 1 in errors are neglected. Under these assumptions, using Eq. (5), the calculated orientation matrix of the crystal on the stage R_{ori} is given by Eq. (10). The ground truth in this situation would be the identity matrix, but the errors result in small nonzero off-diagonal elements.

$$R_{ori} = \begin{bmatrix} 1 & \pm\delta_\varphi \pm\delta_\theta & \pm\delta_\beta \\ \mp\delta_\varphi \mp\delta_\theta & 1 & \pm\delta_\alpha \\ \mp\delta_\beta & \mp\delta_\alpha & 1 \end{bmatrix}. \quad (10)$$

Because of these uncertainties, the calculated angles α_c and β_c to go to another zone axis $[uvw]$ will include errors Δ_α and Δ_β. From the ground truth situation, Eq. (6) yields the expressions in Eq. (11) that apply to the true tilt angles α_c and β_c.

$$\sin\alpha_c = \frac{v}{\sqrt{u^2+v^2+w^2}}, \cos\beta_c = \frac{w}{\sqrt{u^2+w^2}}. \quad (11)$$

Solving the system in Eq. (6) using the perturbed orientation matrix, making the same small angle approximations for sines and cosines as before, and using the ground truth solutions, the errors Δ_α and Δ_β can be derived and are shown in Eq. (12).

$$
\begin{aligned}
|\Delta_\alpha| &= \left| \frac{\pm w\delta_\alpha + u\left(\pm\delta_\theta \pm \delta_\varphi\right)}{\sqrt{u^2 + w^2}} \right| \\
&= \left| \pm\delta_\alpha \cos\beta_c + \left(\pm\delta_\theta \pm \delta_\varphi\right) \sin\beta_c \right|, \\
|\Delta_\beta| &= \left| \pm\delta_\beta + \frac{v\left(\pm\delta_\theta \pm \delta_\varphi\right)}{w} \right| \\
&= \left| \pm\delta_\beta + \frac{\tan\alpha_c}{\cos\beta_c}\left(\pm\delta_\theta \pm \delta_\varphi\right) \right|. \qquad (12)
\end{aligned}
$$

These equations demonstrate that the errors on the calculated angles will be approximately linear functions of the measurement uncertainties but also functions of the tilt angles. If it is assumed that the crystal calibration angle and the detector calibration are the main sources of uncertainty, the errors on the calculated results increase the further the desired zone is from the current zone. If it is assumed these errors combined are on the order of ±0.5–1°, an error of ±0.25–0.5° is expected on both α_c and β_c at the extremes of holder tilt ranges (typically $\alpha = \pm 30^\circ$ and $\beta = \pm 20^\circ$). A very simple starting orientation was considered here and the expressions for the errors will be different when nonzero starting angles are considered. However, the trends and the magnitude on the errors should still hold.

To study the significance of stage nonlinearities and decouple it from the uncertainty in the crystal orientation, a [110] sample of silicon was studied. The crystal orientation with respect to the stage is shown in Figure 7. The $[\bar{1}10]$ zone was found at tilt angles $\alpha = -0.9$ and $\beta = 1.8$. The (002) reflection was measured to be lying at −71° with respect to the detector *X*-axis. Taking an uncertainty on this measurement of ±0.5° and ignoring any detector calibration error, two crystals were created in ALPHABETA representing the uncertainty in the crystal calibration orientation. For these two crystals, the tilt angles to a selection of zones were calculated. The zones are indicated by arrows in Figure 7. These zones were experimentally tilted to and the actual tilt angles as given by the stage to reach perfect zone axis were recorded. All the measured and calculated angles and associated errors are provided in the Supplementary Materials file associated with the electronic version of this paper.

The difference between the calculated stage angles and the measured stage angles at which zones were actually found are plot in Figure 8 both versus the experimental α and β angle. The ends of the error bars represent the calculations performed for the two 'crystals' as described in the previous paragraph. Hence, the error bars represent the uncertainty on the crystal orientation. The error bars widen slightly as tilt angles deviate more from the original orientation, as predicted earlier. However, this uncertainty only represents a small amount of the error, otherwise the points would lie on 0 within the error. There is no clear link between the errors and the α tilt, but there is a clear link between the error and the β tilt: as β deviates from the starting position, the errors significantly deviate from 0°. The error on the α angle remained contained between ±1° within the tested range, but the error on the β angle reached up to ±2°. These errors could not be corrected by adjusting the crystal orientation or detector calibration, which indicates that there is a nonnegligible nonlinear component to the stage tilt, especially when tilting far along the β axis. A total angular error was also calculated, representing the angle between the ideal zone axis and the crystal vector actually found at the calculated tilt angles. Because the error on α is modest, this angle is dominated by the error on β.

These results suggest that, for the stage used in this investigation, when tilting to any arbitrary zone, an accuracy of ±1° on α can be expected, whereas the error on β can reach up to ±2°. These errors are mostly due to stage nonlinearity, particularly in β-tilting; the error due to uncertainty of the crystal orientation contributes only slightly to the overall error. To get the most accurate results for modest tilts to 2-beam and weak beam conditions, the user should tilt to the nearest zone and re-calibrate the crystal orientation using the experimental stage angles. When major β tilts are required to reach a new orientation, the user should be aware of associated errors.

3D dark field

Besides tilting to different zones, a potential application of ALPHABETA is obtaining a 3D view of the sample in dark field or weak beam by tilting around a particular row of reflections. An example where this might be valuable is gaining 3D insight in precipitate distributions (given the precipitates have a systematic orientation relationship with the matrix) using any TEM and any holder. This could be done through stereo pairs or extensive tilt series. The material used in this demonstration contains a fine distribution of TiC nanoprecipitates that are best imaged by the centred dark field (CDF) method using the (200) reflection of TiC, as seen in Figure 9(A). Because the precipitates share the cube-on-cube orientation relationship with the matrix, the matrix reflections can be used for orienting the precipitates. A grain close to the [011] orientation was used to tilt in image mode by increments of 2° around the (200) reflection using calculated α/β values (tilt path shown by the dotted line in the stereographic projection generated by ALPHABETA in Fig. 9B). This allowed keeping (200) reflections excited and obtaining successive dark field images from the nanoprecipitates. Drift was corrected manually by correcting position shift and sample height. Some images are shown in Figure 9(C). The 3D effect is best appreciated when quickly flipping through the images after a drift correction. Such a movie was made and is distributed as supplementary information to the electronic version of this paper. A 3D effect can also be obtained by visually merging the columns in Figure 9(C) by looking at the images slightly cross-eyed.

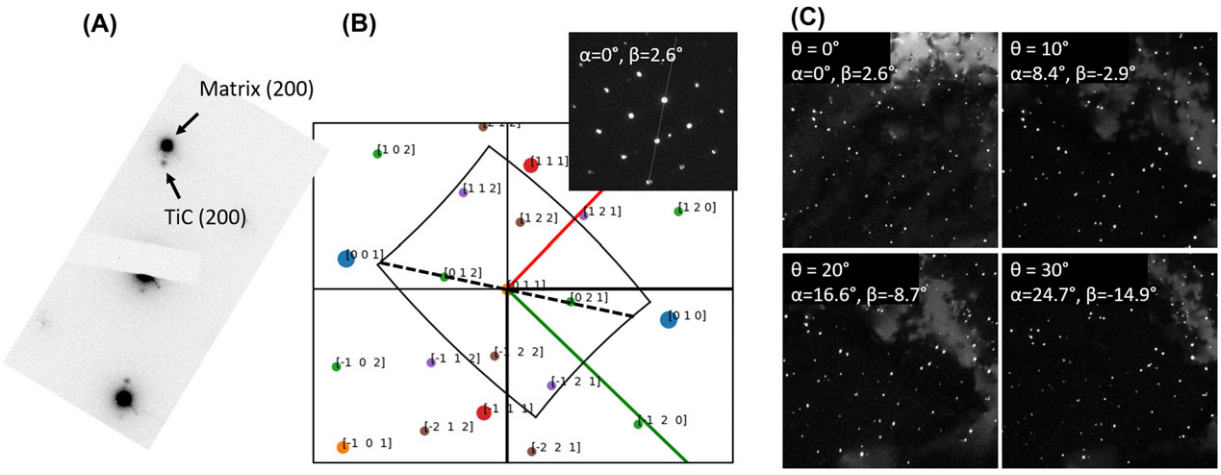

Fig. 9. (A) A diffraction pattern showing the matrix reflection and the TiC (200) reflection from the nanoprecipitates. Due to the cube on cube orientation relationship, these reflections are aligned. (B) The starting situation in the region of interest illustrated with a diffraction pattern and the stereographic projection. The grain was brought to the [011] with a minor beta tilt. The tilt series was taken along the dotted line, around the (200) reflection. (C) The dark field images of approximately the same region at different tilt angles along this path. A 3D illusion can be obtained by looking at the image pairs slightly cross-eyed such that they overlap midway. To provide another visualisation strategy for the 3D illusion, all images taken were put after each other in a Graphics Interchange Formate (GIF) image. This GIF is available as a separate download together with the electronic version of this paper.

Conclusions

The software tool ALPHABETA was developed to assist TEM operators with tilting work. The tool is open source and can be applied to any TEM that has a double tilt stage. Other microscopists might find it useful in their day to day work thanks to its simple user interface, intuitive way to visualise the sample, and its unique combination of tools. This paper described the mathematical framework behind the various calculations the program performs. It also describes the calibrations and conventions used. Over the full tilt range, the error on α should be within $\pm 1°$, whereas the error on β can be slightly larger at $\pm 2°$. The error increases the further the desired orientation is from the original orientation. In the case studied in the paper, the error on the calculation was dominated by stage nonlinearities especially when tilting along β; uncertainty in the original crystal orientation played only a minor role in the error of the result. Besides tilting to different zones, other potential applications include making tilt series around particular reflections. This was demonstrated for dark field imaging of Ti–C nanoprecipitates.

References

Bajd, T., Mihelj, M. & Munih, M. (2013) Rotation and orientation. *Introduction to Robotics*, 1st ed., pp. 9–35. Springer, the Netherlands.

'CrystalPack Module'. (2017) Thermo Scientific. https://www.fei.com/document/crystalpack-module-app-note.pdf.

Duden, T., Gautam, A. & Dahmen, U. (2011) KSpaceNavigator as a tool for computer-assisted sample tilting in high-resolution imaging, tomography and defect analysis. *Ultramicroscopy* **111**(11), 1574–1580.

Graef, M.De. & McHenry, M.E. (2007) *Structure of Materials: An Introduction to Crystallography, Diffraction and Symmetry*. Cambridge University Press, Cambridge, UK.

Jenkins, M.L. & Kirk, M.A. (2000) *Characterisation of Radiation Damage by Transmission Electron Microscopy*. Series in Microscopy in Materials Science, Taylor & Francis, Boca Raton.

Klinger, M. & Jäger, A. (2015) Crystallographic tool box (CrysTBox): automated tools for transmission electron microscopists and crystallographers. *J. Appl. Crystallogr.* **48**(2015), 2012–2018.

'Mel-Build'. (2005) http://www.melbuild.com/.

Midgley, P.A. & Dunin-Borkowski, R.E. (2009) Electron tomography and holography in materials science. *Nat. Mater.* **8**, 271–280.

Weyland, M. & Midgley, P.A. (2004) Electron tomography. *Mater. Today* **7**(12), 32–40.

Supporting Information

Additional supporting information may be found online in the Supporting Information section at the end of the article.

1. A note on beam sensitive materials
2. Calibrating the detector
3. Tilting to a new zone (additional examples)